JPE 16-6-1

http://dx.doi.org/10.6113/JPE.2016.16.6.1991
ISSN(Print): 1598-2092 / ISSN(Online): 2093-4718

Single-Phase Improved Auxiliary Resonant Snubber Inverter that Reduces the Auxiliary Current and THD

Hailin Zhang†, Baoquan Kou*, He Zhang*, and Lu Zhang*

†,*Department of Electrical Engineering, Harbin Institute of Technology, Harbin, China

Abstract

An LC filter is required to reduce the output current ripple in the auxiliary resonant snubber inverter (ARSI) for high-performance applications. However, if the traditional control method is used in the ARSI with LC filter, then unnecessary current flows in the auxiliary circuit. In addressing this problem, a novel load-adaptive control that fully uses the filter inductor current ripple to realize the soft-switching of the main switches is proposed. Compared with the traditional control implemented in the ARSI with LC filter, the proposed control can reduce the required auxiliary current, contributing to higher efficiency and DC-link voltage utilization. In this study, the detailed circuit operation in the light load mode (LLM) and the heavy load mode (HLM) considering the inductor current ripple is described. The characteristics of the improved ARSI are expressed mathematically. A prototype with 200 kHz switching frequency, 80 V DC voltage, and 8 A maximum output current was developed to verify the effectiveness of the improved ARSI. The proposed ARSI was found to successfully operate in the LLM and HLM, achieving zero-voltage switching (ZVS) of the main switches and zero-current switching (ZCS) of the auxiliary switches from zero load to full load. The DC-link voltage utilization of the proposed control is 0.758, which is 0.022 higher than that of the traditional control. The peak efficiency is 91.75% at 8 A output current for the proposed control, higher than 89.73% for the traditional control. Meanwhile, the carrier harmonics is reduced from –44 dB to –66 dB through the addition of the LC filter.

Key words: Auxiliary resonant snubber inverter, Soft-switching, Zero-voltage switching (ZVS), Zero-current switching (ZCS)

I. INTRODUCTION

In integrated circuit manufacturing, electromechanical actuators, such as voice coil motors and permanent magnet linear motors, are used to drive the wafer stage and the reticle stage to accomplish exposure, dicing, inspection, or other handling tasks [1]. These systems must operate with high dynamic response and nanometer-position error range. Inverters are used to provide the output currents to drive the actuators. To achieve the high performance of the systems, inverters must meet the requirements of high bandwidth and high linearity. Thus, high switching frequency is the least important requirement for inverters. However, as the switching frequency increases to hundreds of kHz, large switching loss and severe electromagnetic interference (EMI) occur [2], [3].

In solving the problems of large switching loss and severe EMI in a high switching frequency inverter, the soft-switching technique is one of the best options. The switching loss and EMI noise are reduced by limiting the di/dt or dv/dt during the commutation process. To date, various soft-switching DC–AC topologies have been proposed. Among them, the zero-voltage-switching (ZVS) resonant pole inverter (RPI) [4]-[20] has been well-accepted because of its simple control strategy and soft-switching operation over a wide load range.

Auxiliary resonant snubber inverter (ARSI) is a type of ZVS RPI [4], [5]. ARSI has an auxiliary circuit placed between different phase-leg and resonant capacitors connected in parallel to the main switches. Compared with the hysteresis current-controlled RPI [6], [7], ARSI can achieve ZVS from zero load to full load and use pulse-width modulation (PWM) at a fixed switching frequency. Compared with the auxiliary resonant commutated pole inverter (ARCPI) [8], [9], ARSI eliminates the split capacitors and solves the voltage imbalance problems. Compared with other zero-voltage-transition topologies [10]-[15], the auxiliary circuit and the control scheme are simpler. The disadvantage of ARSI is that the three-phase ARSI cannot use the conventional space-vector

Manuscript received Feb. 7, 2016; accepted Jun. 24, 2016
Recommended for publication by Associate Editor Il-Oun Lee.
†Corresponding Author: zhanghailin0310@sina.com
Tel: +86-451-86403003, Harbin Institute of Technology
*Dept. of Electrical Engineering, Harbin Institute of Technology, China

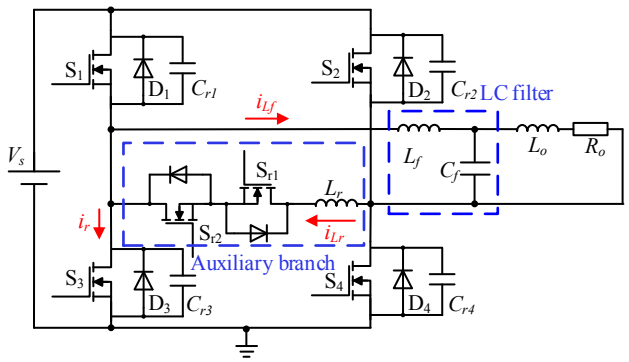

Fig. 1. Improved ARSI with LC filter.

pulse-width modulation (SVPWM), which makes it more suitable for permanent magnet brushless DC motors instead of all types of motors [4]. However, no such drawback is observed in the single-phase topology. In addition, the single-phase ARSI has a significantly simple auxiliary circuit, with only two auxiliary switches and one resonant inductor.

Many previous studies on ARSI have focused on the control strategy to improve efficiency [16]-[20]. Instead of fixed-timing control, variable timing control has been proposed to improve efficiency [16], [17]. In further improving efficiency, a control scheme of natural ZVS (NZVS), in which the auxiliary resonant circuit is used in only a half cycle, has been proposed [18]. Next, an adjustable dead-time control has been proposed to solve the NZVS problem; however, this approach leads to large harmonic distortion because of the large amount of dead time near the zero output current range [19]. In addressing this issue, a dead-time compensation scheme has been proposed to reduce harmonic distortion [20].

Previous studies aimed to improve efficiency without regarding output quality. However, when the ARSI is applied to high-performance motor drive applications, an output filter, such as an LC filter, must be added to address the problem of large output current ripple. In avoiding influencing the system's stability, the cut-off frequency of the filter should be higher than the bandwidth [21]. This requirement leads to relatively high filter inductor current ripple. With the traditional analysis and control, the inductor current ripple is neglected [16]-[20]. In this case, if the traditional control is still used in the circuit with an LC filter, then extra current flows in the auxiliary circuit, resulting in high conduction loss and low DC-link voltage utilization.

In addressing the problem, a novel load-adaptive control of the improved ARSI that fully uses the filter inductor current ripple to realize the soft-switching of the main switches is proposed. Compared with the features of the traditional control used in the ARSI with LC filter, the major improvements of the proposed control are stated as follows: 1) the required auxiliary current is reduced; 2) the loss is lower and the efficiency is improved through the reduction of the auxiliary current; and 3) the DC-link voltage utilization is improved through the reduction of the conduction time of the auxiliary circuit.

The paper is organized as follows. In Section II, two operating modes of the improved ARSI are analyzed. In Section III, the features and characteristics are discussed. In Section IV, the design guideline is introduced. In Section V, the control scheme is presented. A hardware prototype is designed and tested. The experimental results of the traditional control and the proposed control used in the improved ARSI are compared.

II. Basic Topology and Operating Principle

Fig. 1 shows the circuit of the improved ARSI, which consists of a standard H-bridge inverter, an auxiliary branch, and an LC filter.

The improved ARSI operates in two modes, namely, heavy load mode (HLM) and light load mode (LLM), as determined by the state of the filter inductor current. The detailed circuit operation of the LLM and the HLM are analyzed in the case of positive output current. The following are assumed:

1) All components and devices are ideal.

2) The gate signals of the MOSFETs are ideal square-waves.

3) The output inductor L_o is high enough to be a constant current source.

A. LLM

One switching cycle of the operating waveforms and operating stages in the LLM are shown in Fig. 2 and Fig. 3, where v_{ds} is the drain–source voltage of a MOSFET, i_d is the drain current of a MOSFET, v_g is the gate signal, i_{Lf} is the filter inductor current, and i_{Lr} is the resonant inductor current.

1) Stage a [t_{L0}-t_{L1}]: This stage is the initial condition where S_1 and S_4 are in the on state and S_2 and S_3 are in the off state. A positive load current flows through S_1 and S_4. The filter inductor current i_{Lf} increases linearly in the positive direction with positive voltage V_s.

2) Stage b [t_{L1}-t_{L2}]: With the resonant capacitors C_{r1} and C_{r4}, v_{ds1} and v_{ds4} increase very slowly. Therefore, S_1 and S_4 are turned off at ZVS at t_{L1}. Subsequently, all the main switches are in off states, and the filter inductor begins resonating with four resonant capacitors. C_{r2} and C_{r3} are discharged and C_{r1} and C_{r4} are charged because of the direction of the resonant current. The resonant time is very short, and the inductance L_f is high. Therefore, the filter current is considered to be constant during the resonant time. Thus, the drain–source voltages of the MOSFETs can be expressed as follows:

$$v_{ds1}(t) = v_{ds4}(t) = \frac{i_{Lf\_u}}{2C_r}(t - t_{L1}) \quad (1)$$

$$v_{ds2}(t) = v_{ds3}(t) = V_s - \frac{i_{Lf\_u}}{2C_r}(t - t_{L1}) \quad (2)$$

When v_{ds2} and v_{ds3} decrease to zero at t_{L2}, the resonant period is complete. The resonant time is calculated as follows:

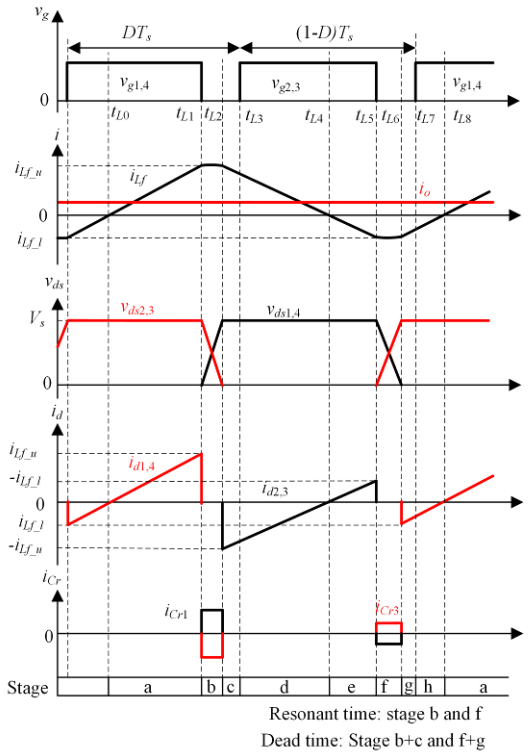

Fig. 2. Voltage and current waveforms in the LLM.

$$\Delta t_{L12} = t_{L2} - t_{L1} = \frac{2C_r V_s}{i_{Lf\_u}} \tag{3}$$

3) Stage c [t_{L2}-t_{L3}]: After C_{r2} and C_{r3} are discharged to zero voltage, the body diodes D_2 and D_3 conduct the current. Next, the voltage of the filter inductor L_f becomes negative, causing i_{Lf} to decrease linearly.

4) Stage d [t_{L3}-t_{L4}]: With the conduction of D_2 and D_3, v_{ds2} and v_{ds3} remain as zero. Therefore, S_2 and S_3 are zero voltage turned on at t_{L3}. The current is diverted from the body diodes to the MOSFET channels, which operate in the third quadrant. Meanwhile, i_{Lf} decreases linearly with negative voltage V_s.

5) Stage e [t_{L4}-t_{L5}]: i_{Lf} drops to zero at t_{L4} and then increases in the negative direction. Therefore, MOSFETs S_2 and S_3 begin operating in the first quadrant because of the negative filter inductor current.

6) Stage f [t_{L5}-t_{L6}]: S_2 and S_3 are turned off at the ZVS condition at t_{L5}. Subsequently, the filter inductor begins resonating with the resonant capacitors. With the negative filter inductor current, C_{r2} and C_{r3} are charged and C_{r1} and C_{r4} are discharged during this resonant period. The drain–source voltages of the MOSFETs can be expressed as follows:

$$v_{ds1}(t) = v_{ds4}(t) = V_s + \frac{i_{Lf\_l}}{2C_r}(t - t_{L5}) \tag{4}$$

$$v_{ds2}(t) = v_{ds3}(t) = -\frac{i_{Lf\_l}}{2C_r}(t - t_{L5}) \tag{5}$$

v_{ds1} and v_{ds4} decrease to zero at t_{L6}. At this point, the resonant period is complete, and the period can be calculated.

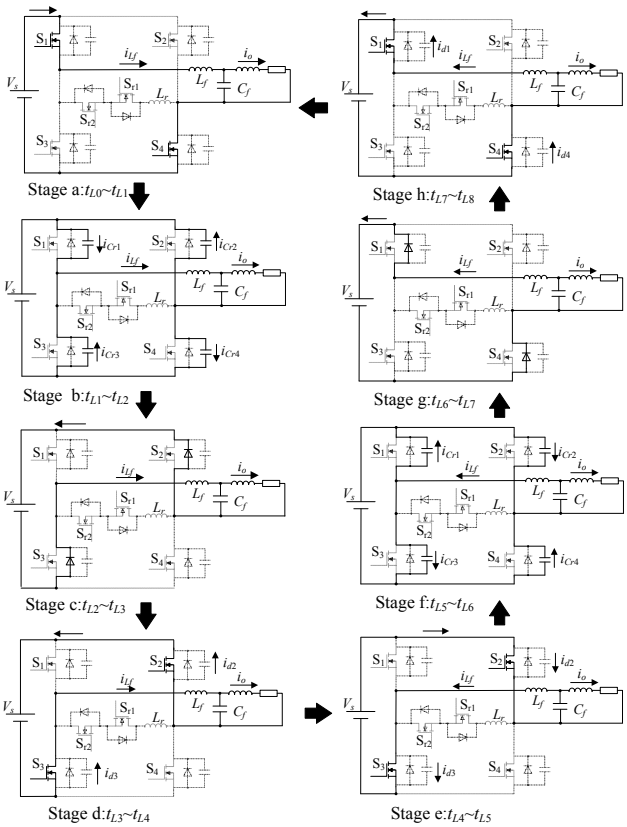

Fig. 3. Operation stages in the LLM.

$$\Delta t_{L56} = t_{L6} - t_{L5} = -\frac{2C_r V_s}{i_{Lf\_l}} \tag{6}$$

7) Stage g [t_{L6}-t_{L7}]: After v_{ds1} and v_{ds4} decrease to zero, the body diodes D_1 and D_4 conduct the negative filter inductor current.

8) Stage h [t_{L7}-t_{L8}]: The conduction of the diodes keep v_{ds1} and v_{ds4} at zero. Thus, the switches S_1 and S_4 are turned on at the ZVS condition and then operate in the third quadrant.

B. HLM

As the output current increases, the filter inductor current cannot generate the ZVS condition for all the main switches because the current is not high enough to discharge the resonant capacitors to zero voltage or because the direction of the current is not appropriate during the resonant period. Therefore, the auxiliary switches S_{r1} and S_{r2} are turned on properly in the HLM. Fig. 4 and Fig. 5 illustrate the detailed operation waveforms and operating stages in the positive load current condition in the HLM. Stages A–D are similar to those in the LLM, in which S_2 and S_3 achieve ZVS with filter inductor current i_{Lf}. Therefore, the operation principle is described starting with stage E as follows.

1) Stage E [t_{H4}-t_{H5}]: S_{r1} is turned on at the zero-current-switching (ZCS) condition at t_{H4} because of resonant inductor L_r. Subsequently, the resonant inductor current i_{Lr} increases linearly.

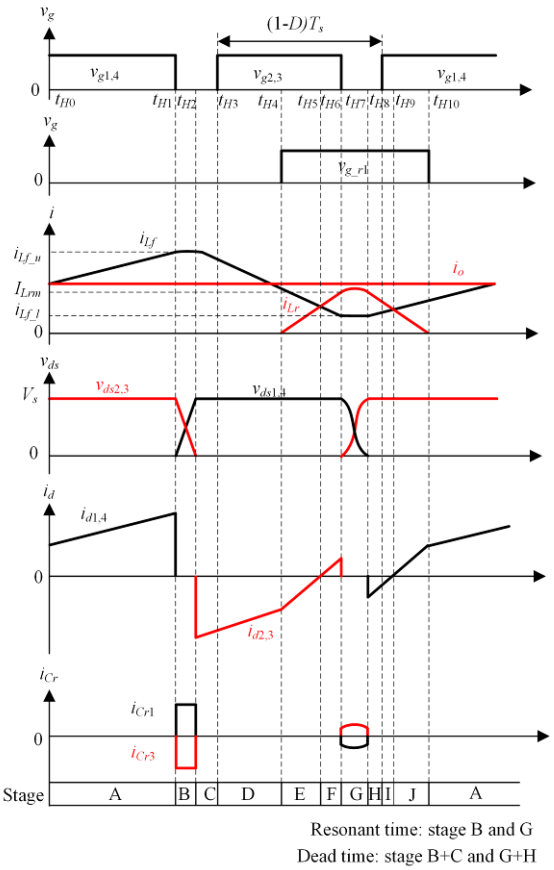

Fig. 4. Voltage and current waveforms in the HLM.

$$i_{Lr}(t)=\frac{V_s}{L_r}(t-t_{H4}) \tag{7}$$

Meanwhile, i_{Lf} decreases linearly. As the differences between i_{Lf} and i_{Lr}, i_{d2} and i_{d3} decrease in the negative direction.

$$i_{d2}=i_{d3}=-i_{Lf}+i_{Lr} \tag{8}$$

2) Stage F [t_{H5}-t_{H6}]: i_{Lf} equals i_{Lr} at t_{H5}, resulting in i_{d2} and i_{d3} decreasing to zero. Thus, S_2 and S_3 operate in the first quadrant. i_{d2} and i_{d3} increase in the positive direction. These currents obey Equs. (7)-(8).

3) Stage G [t_{H6}-t_{H7}]: The resonant inductor is charged to I_{Lrm} at t_{H6}. Meanwhile, S_2 and S_3 are turned off at the ZVS condition at t_{H6}. Thus, the resonant capacitors resonate with L_r and L_f. The filter inductance is significantly higher than resonant inductance $L_f > L_r$ and the resonant time is very short. Therefore, the filter inductor current is considered to be constant $i_{Lf}(t) = i_{Lf\_l}$. C_{r1} and C_{r4} are discharged and C_{r2} and C_{r3} are charged because of the direction of the initial resonant current. The equations during this resonant period can be written as follows:

$$v_{ds1}(t)+v_{ds3}(t)=V_s \tag{9}$$

$$i_{cr1}(t)=C_r\frac{dv_{ds1}(t)}{dt} \tag{10}$$

$$i_{cr3}(t)=C_r\frac{dv_{ds3}(t)}{dt} \tag{11}$$

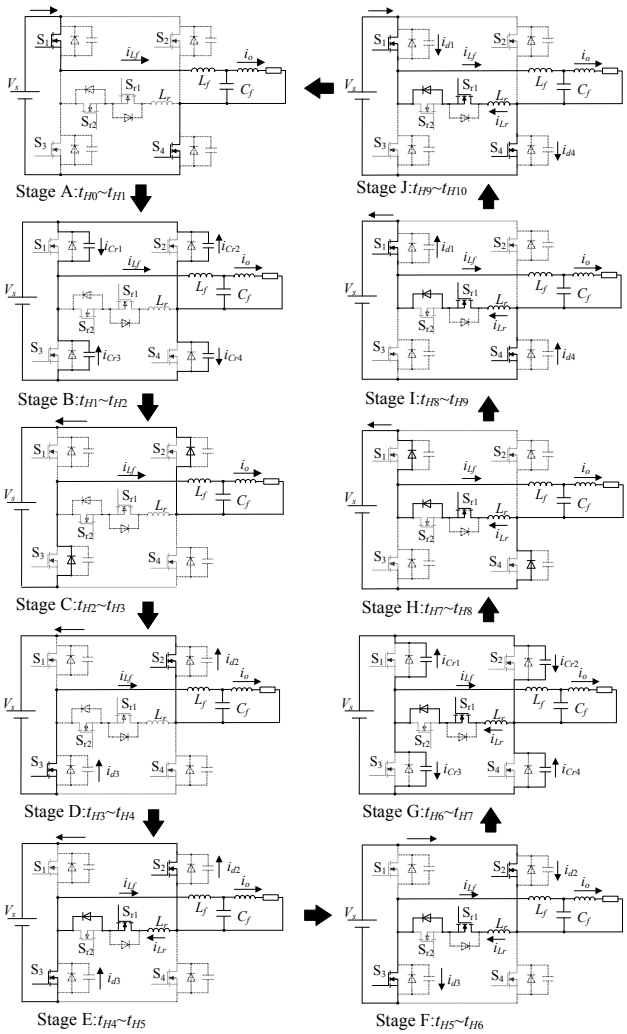

Fig. 5. Operation stages in the HLM.

$$i_{cr1}(t)+i_{Lr}(t)=i_{Lf\_l}+i_{cr3}(t) \tag{12}$$

$$v_{ds1}(t)-v_{ds3}(t)=L_r\frac{di_{Lr}(t)}{dt} \tag{13}$$

The initial conditions are shown as follows:

$$v_{ds1}(t_{H6})=v_{ds4}(t_{H6})=V_s \tag{14}$$

$$v_{ds2}(t_{H6})=v_{ds3}(t_{H6})=0 \tag{15}$$

$$i_{Lr}(t_{H6})=I_{Lrm} \tag{16}$$

Therefore, the parameters can be described as:

$$\begin{aligned} i_{Lr}(t)=&\left(I_{Lrm}-i_{Lf\_l}\right)\cos\omega_A(t-t_{H6})\\ &+\frac{V_s}{Z_A}\sin\omega_A(t-t_{H6})+i_{Lf\_l}\end{aligned} \tag{17}$$

$$\begin{aligned} v_{ds1}(t)=v_{ds4}(t)=&\frac{1}{2}V_s+\frac{1}{2}V_s\cos\omega_A(t-t_{H6})\\ &-\frac{1}{2}Z_A\left(I_{Lrm}-i_{Lf\_l}\right)\sin\omega_A(t-t_{H6})\end{aligned} \tag{18}$$

$$\begin{aligned} v_{ds2}(t)=v_{ds3}(t)=&\frac{1}{2}V_s-\frac{1}{2}V_s\cos\omega_A(t-t_{H6})\\ &+\frac{1}{2}Z_A\left(I_{Lrm}-i_{Lf\_l}\right)\sin\omega_A(t-t_{H6})\end{aligned} \tag{19}$$

$$i_{Cr1}(t)=i_{Cr4}(t)=-\frac{V_s}{2Z_A}\sin\omega_A(t-t_{H6}) -\frac{1}{2}\left(I_{Lrm}-i_{Lf\_l}\right)\cos\omega_A(t-t_{H6}) \quad (20)$$

$$i_{Cr2}(t)=i_{Cr3}(t)=\frac{V_s}{2Z_A}\sin\omega_A(t-t_{H6}) +\frac{1}{2}\left(I_{Lrm}-i_{Lf\_l}\right)\cos\omega_A(t-t_{H6}) \quad (21)$$

where $\omega_A=\frac{1}{\sqrt{L_rC_r}}$, $Z_A=\sqrt{\frac{L_r}{C_r}}$, and I_{Lrm} is the initial resonant inductor current.

For $v_{ds1}(t) = 0$, the resonant time can be calculated as:

$$\Delta t_{H67}=t_{H7}-t_{H6}=\frac{2}{\omega_A}\arcsin\frac{V_s}{\sqrt{V_s^2+Z_A^2(I_{Lrm}-i_{Lf\_l})^2}} \quad (22)$$

At the end of the resonant time t_{H7}, i_{Lr} can be obtained.

$$i_{Lr}(t_{H7})=I_{Lrm} \quad (23)$$

4) Stage H [t_{H7}-t_{H8}]: The resonant period is complete at t_{H7} when v_{ds1} and v_{ds4} decrease to zero. Thus, D_1 and D_4 conduct the current. In addition, the filter inductor current i_{Lf} increases, and i_{Lr} decreases.

$$i_{Lr}(t)=i_{Lr}(t_{H7})-\frac{V_s}{L_r}(t-t_{H7})=I_{Lrm}-\frac{V_s}{L_r}(t-t_{H7}) \quad (24)$$

5) Stage I [t_{H8}-t_{H9}]: v_{ds1} and v_{ds4} are kept at zero because of the conduction of the diodes. Thus, S_1 and S_4 are turned on at the ZVS condition at t_{H8}. The current is diverted from D_1 and D_4 to the channels of MOSFETs S_1 and S_4. Meanwhile, i_{Lf} still increases, and i_{Lr} decreases.

6) Stage J [t_{H9}-t_{H10}]: The resonant inductor current i_{Lr} still decreases linearly and decreases to zero at t_{H10}. Thus, S_{r1} is turned off at the ZCS condition.

III. Analysis of Features and Characteristics

A. Soft-switching condition in LLM and HLM

The analysis of the operation principle in Section II shows that regardless of whether the inverter operates in the LLM or HLM, the direction of the initial resonant current I_r should enable the resonant capacitors that are parallel to the next turn-on MOSFET to be discharged. To achieve NZVS, the auxiliary circuit is not operated. The filter inductor current i_{Lf} provides the initial resonant current I_r. In achieving auxiliary ZVS (AZVS), the auxiliary circuit is conducted, and I_r is the difference between i_{Lr} and i_{Lf} at the beginning of the resonant time.

Meanwhile, in achieving the ZVS of the main switches, the magnitude of the initial resonant current should be high enough so that the resonant capacitors can be discharged to zero-voltage during the dead time. Therefore, the resonant time should be shorter than the dead time.

$$t_r<t_{dead} \quad (25)$$

According to Equs. (3) and (6), the resonant time for achieving NZVS can be calculated as follows:

$$t_r=\frac{2C_rV_s}{I_r} \quad (26)$$

Equs. (25) and (26) show that I_r must meet the following requirement to achieve NZVS.

$$I_r>\frac{2C_rV_s}{t_{dead}}=I_{r\_\min} \quad (27)$$

Section II mentioned that I_r is related to the upper or lower envelopes of the filter inductor currents i_{Lf_u} and i_{Lf_l} in each resonant period. The positive i_{Lf_u} helps S_2 & S_3 achieve ZVS, and the negative i_{Lf_l} provides the ZVS condition for S_1 & S_4. As a result, if i_{Lf_u} and i_{Lf_l} meet the requirements $i_{Lf\_u} > I_{r\_\min}$ and $i_{Lf\_l} < -I_{r\_min}$, then all the main switches can achieve NZVS without the operation of the auxiliary circuit. Otherwise, the inverter operates in the HLM. A set of switches achieve AZVS with the operation of the auxiliary circuit.

According to Equ. (22), the resonant time for achieving AZVS can be obtained as follows:

$$t_r=\frac{2}{\omega_A}\arcsin\frac{V_s}{\sqrt{V_s^2+Z_A^2I_r^2}} \quad (28)$$

Equs. (25) and (28) show that I_r must meet the following requirement to achieve AZVS.

$$I_r>\frac{V_s}{Z_A}\frac{1}{\left|\tan\frac{\omega_At_{dead}}{2}\right|} \quad (29)$$

S_{r1} is turned on to realize the AZVS of S_1 and S_4 when the output current is positive. S_{r2} is turned on to generate the ZVS condition for S_2 and S_3 when the output current is negative. Table I shows the ZVS condition of the LLM and the HLM.

Moreover, the energy of inductors L_f and L_r must be high enough to ensure that the resonant capacitors are discharged to zero voltage. Therefore, in achieving NZVS, the energy of the filter inductor must meet the following requirement:

$$\frac{1}{2}L_fI_r^2>4\times\frac{1}{2}C_rV_s^2=2C_rV_s^2 \quad (30)$$

According to Equ. (7) in [18], the energy of the resonant inductor must meet the following requirement to achieve AZVS in the HLM:

$$\frac{1}{2}L_rI_r^2>2C_rV_s^2 \quad (31)$$

B. Lower Peak Current Stress of the Auxiliary Switch and Shorter ON Time

In the heavy load condition, the auxiliary circuit must be operated to obtain an initial resonant current I_r that meets the soft-switching condition to achieve the AZVS of the main switches. When the output current is positive as shown by the analysis in Section II, S_{r1} is turned on before S_2 & S_3 are turned off to obtain a proper I_r to achieve the AZVS of S_1 & S_4.

TABLE I
ZVS TYPES OF SWITCHES FOR DIFFERENT OUTPUT CURRENTS

	$i_{Lf\_l} < i_{Lf\_u} < I_{r\_min}$	$i_{Lf\_u} > I_{r\_min}$ and $i_{Lf\_l} < -I_{r\_min}$	$i_{Lf\_u} > i_{Lf\_l} > -I_{r\_min}$
S_1,S_4	NZVS	NZVS	AZVS(S_{r1})
S_2,S_3	AZVS(S_{r2})	NZVS	NZVS
Mode	HLM	LLM	HLM

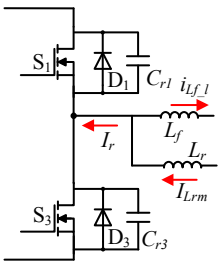

Fig. 6. Circuit at the beginning of the resonant time.

Fig. 6 shows the circuit condition at the beginning of the resonant time in the case of positive load current. The initial resonant current I_r is the difference between the initial resonant inductor current I_{Lrm} and the lower envelope of resonant current i_{Lf_l}. Thus, the required I_{Lrm} can be calculated as follows:

$$I_{Lrm} = i_{Lf\_l} + I_r \tag{32}$$

I_r is constant in achieving AZVS, whereas i_{Lf_l} changes as the load current changes. In obtaining a constant I_r, I_{Lrm} should follow i_{Lf_l} adaptively according to Equ. (32). For i_{Lf_l}, it is related to the output voltage. Fig. 2 and Equs. (1)-(6) show that the output voltage in the LLM can be obtained as:

$$\begin{aligned} v_{o\_L} &= \frac{1}{T_s}\int_{t_{L0}}^{t_{L8}} (v_{ds3} - v_{ds4})dt \\ &= [(2D-1) + \frac{\Delta t_{L56} - \Delta t_{L12}}{T_s}]V_s \\ &= (2D-1)V_s + (\frac{2C_rV_s}{|i_{Lf\_l}|} - \frac{2C_rV_s}{|i_{Lf\_u}|})\frac{V_s}{T_s} \end{aligned} \tag{33},$$

where D is the duty ratio, and T_s is the switching period.

The resonant times Δt_{L12} and Δt_{L56} are very short, and their values are close to each other. Therefore, the output voltage in the LLM is close to:

$$v_{o\_L} \approx (2D-1)V_s \tag{34}$$

From Fig. 4 and Equs. (1)–(3), (18), (19), and (22), the output voltage in the HLM can be obtained as:

$$\begin{aligned} v_{o\_H} &= \frac{1}{T_s}\int_{t_0}^{t_9} (v_{ds3} - v_{ds4})dt \\ &= [(2D-1) + \frac{\Delta t_{H67} - \Delta t_{H12}}{T_s}]V_s \\ &= (2D-1)V_s + (\frac{2}{\omega_A}\arcsin\frac{V_s}{\sqrt{V_s^2 + Z_A^2 I_r^2}} - \frac{2C_rV_s}{|i_{Lf\_u}|})\frac{V_s}{T_s} \end{aligned} \tag{35}$$

The resonant times Δt_{H12} and Δt_{H67} are very short, and their values are close to each other. Therefore, the output voltage in the HLM is close to:

$$v_{o\_H} \approx (2D-1)V_s \tag{36}$$

Thus, the output current from zero load to full load is calculated as follows:

$$v_o = (2D-1)V_s \tag{37}$$

The filter inductor current ripple can be calculated as:

$$\Delta i_{Lf} = \frac{V_s - v_o}{L_f}DT_s = \frac{(2-2D)DV_sT_s}{L_f} \tag{38}$$

The average filter inductor current in each switching cycle equals the output current. Thus, the envelope of the filter inductor currents i_{Lf_u} and i_{Lf_l} are given by the following:

$$i_{Lf\_u} = i_o + \frac{1}{2}\Delta i_{Lf} = i_o + \frac{(1-D)DV_sT_s}{L_f} \tag{39}$$

$$i_{Lf\_l} = i_o - \frac{1}{2}\Delta i_{Lf} = i_o - \frac{(1-D)DV_sT_s}{L_f} \tag{40}$$

From Equs. (32) and (40), the required initial resonant inductor current can be obtained as follows:

$$I_{Lrm} = |i_o| + I_r - \frac{(1-D)DV_sT_s}{L_f} \tag{41}$$

Fig. 7 shows the on time of the auxiliary switch involving the charging time t_{ch}, the resonant time t_r, and the discharging time t_{dch}. The charging time determines the turn-on moment of the auxiliary switches and the magnitude of i_{Lr}. Therefore, in obtaining I_{Lrm}, the charging time of the resonant inductor is given by the following:

$$t_{ch} = \frac{L_rI_{Lrm}}{V_s} = \frac{(|i_o| + I_r)L_r}{V_s} - \frac{(1-D)DT_sL_r}{L_f} \tag{42}$$

Equs. (7) and (24) show that the discharging time equals the charging time. Therefore, the on time of the resonant inductor can be obtained as follows:

$$t_A = t_{ch} + t_r + t_{dch} = 2t_{ch} + t_r \tag{43}$$

When the output current is negative ($i_o < 0$), Equs. (41)–(43) are also correct.

For the traditional control, the current ripple is not considered. The average filter inductor current in one switching cycle equals i_o. Therefore, the resonant inductor current must be charged to I_{Lrm_t} to obtain the initial resonant current I_r as follows, according to Equ. (32).

$$I_{Lrm\_t} = |i_o| + I_r \tag{44}$$

The charging time of the resonant inductor in the traditional control can be given by the following equation:

$$t_{ch\_t} = \frac{L_ri_{Lrm\_t}}{V_s} = \frac{(|i_o| + I_r)L_r}{V_s} \tag{45}$$

Fig. 7 shows the required auxiliary current of the ARSI with traditional control and the proposed control during the on interval of the auxiliary branch. According to Equs. (41)–(45), because the proposed control fully uses the filter inductor current ripple, the initial resonant inductor current is $\Delta i_{Lf}/2$ lower than that of the traditional control, resulting in a

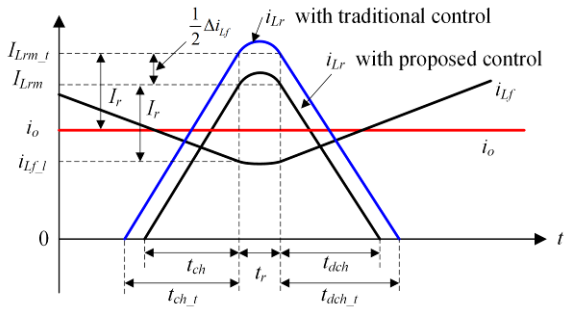

Fig. 7. Waveforms during the on interval of the auxiliary branch.

reduced peak current stress of the auxiliary switch. In addition, the charging time of the resonant inductor is $\Delta i_{Lf} L_r / 2V_s$, that is, shorter.

C. High DC-Link Voltage Utilization

Fig. 8 shows the dynamic response waveforms when the output current increases from zero to the maximum value. During the rise time of the output current, the inverter operates at the maximum duty ratio D_{max}. Initially, the circuit operates in the LLM because $i_{Lf\_l} < -I_{r\_min}$, which can realize the NZVS of the main switches. When $i_{Lf\_l} > -I_{r\_min}$, the inverter switches to HLM, in which S_{r1} is turned on during the conduction time of S_2 and S_3 to charge the resonant inductor in the positive direction. Thus, the initial resonant current I_r can be obtained to make S_1 and S_4 achieve AZVS. Therefore, the on time of S_2 and S_3 must be longer than the charging time of the resonant inductor.

$$t_{S2\_on} > t_{ch} \tag{46}$$

The maximum duty ratio D_{max} is determined by the minimum on time of S_2 and S_3 ($t_{S2\_on\_min}$). Moreover, $t_{S2\_on\_min}$ is determined by the maximum charging time of the resonant inductor t_{ch_max}. When the output current increases to the maximum with D_{max} in Fig. 8, the required initial resonant inductor current reaches its maximum value I_{Lrm_max}, resulting in the maximum charging time of the resonant inductor. From Equ. (42), the maximum charging time of the resonant inductor is given by the following equation:

$$t_{ch\_\max} = \frac{(I_{o\_\max} + I_r)L_r}{V_s} - \frac{(1 - D_{\max})D_{\max} T_s L_r}{L_f} \tag{47}$$

The minimum on time of S_2 and S_3 is calculated as follows:

$$t_{S2\_on\_\min} = (1 - D_{\max})T_s - t_{dead} \tag{48}$$

where t_{dead} is the dead time.

Therefore, for $t_{S2\_on\_min} = t_{ch\_max}$, D_{max} is calculated as:

$$D_{\max} = \frac{-b + \sqrt{b^2 - 4ac}}{2a} \tag{49}$$

where $a = V_s T_s L_r$

$$b = (L_f - L_r)V_s T_s$$

$$c = (I_r + I_{o\_\max})L_r L_f - (T_s - t_{dead})V_s L_f$$

For the ARSI with traditional control, the maximum duty ratio can be obtained from Equ. (44) as follows:

$$D_{\max\_t} = 1 - \frac{(I_{o\_\max} + I_r)L_r}{V_s T_s} - \frac{t_{dead}}{T_s} \tag{50}$$

From the analysis above, the maximum resonant inductor current I_{Lrm_max} determines the maximum charging time of resonant inductor t_{ch_max}. In addition, t_{ch_max} determines the maximum duty ratio D_{max}. With lower required auxiliary current of the improved ARSI for the proposed control shown in Fig.7, the maximum duty ratio is higher than that for the traditional control.

The DC-link voltage utilization is the ratio between the maximum output voltage and DC voltage. According to Equ. (36), the DC-link voltage utilization η_{dc} can be obtained through the following equation:

$$\eta_{dc} = \frac{v_{o\_\max}}{V_s} = 2D_{\max} - 1 \tag{51}$$

With the operation of the auxiliary circuit, D_{max} and DC-link voltage utilization are limited, which is the drawback of the ARSI compared with the hard-switching inverter. The analysis above shows that because the proposed control uses the current ripple, the required auxiliary current is reduced, and the maximum duty cycle is greater than that of the traditional control. Therefore, the DC-link voltage utilization η_{dc} is improved. As a result, a lower DC voltage can be used to accomplish the same performance with a higher DC voltage utilization. Moreover, a high di_o/dt related to the jerk of the motor can be obtained under the same DC voltage with a better DC voltage utilization.

IV. DESIGN GUIDELINE

The input and output data specifications are the following: DC voltage V_s = 80 V, switching frequency f_s = 200 kHz, and maximum output current I_{o_max} = 8 A. The design procedure of the improved ARSI is described as follows.

Step 1) Design the LC filter

The LC filter is used to attenuate the high frequency harmonics, but the bandwidth of the improved ARSI should not be reduced. Thus, a trade-off exists between the attenuation effect and the system bandwidth.

$$2f_b \le f_{\mathrm{LC}} \le \frac{1}{5} f_s \tag{52}$$

The bandwidth of the improved ARSI is specified as f_b = 10 kHz. Therefore, the cut-off frequency of the LC filter is selected as $f_{LC} = 3f_b$ = 30 kHz.

$$\frac{1}{2\pi\sqrt{L_f C_f}} = 30000 \tag{53}$$

In optimizing the transient performance, the filter ratio is given as follows, according to [21].

$$\frac{Z_o}{e^{\xi_c}} \le \sqrt{\frac{L_f}{C_f}} \le \frac{Z_o}{\xi_c} \tag{54}$$

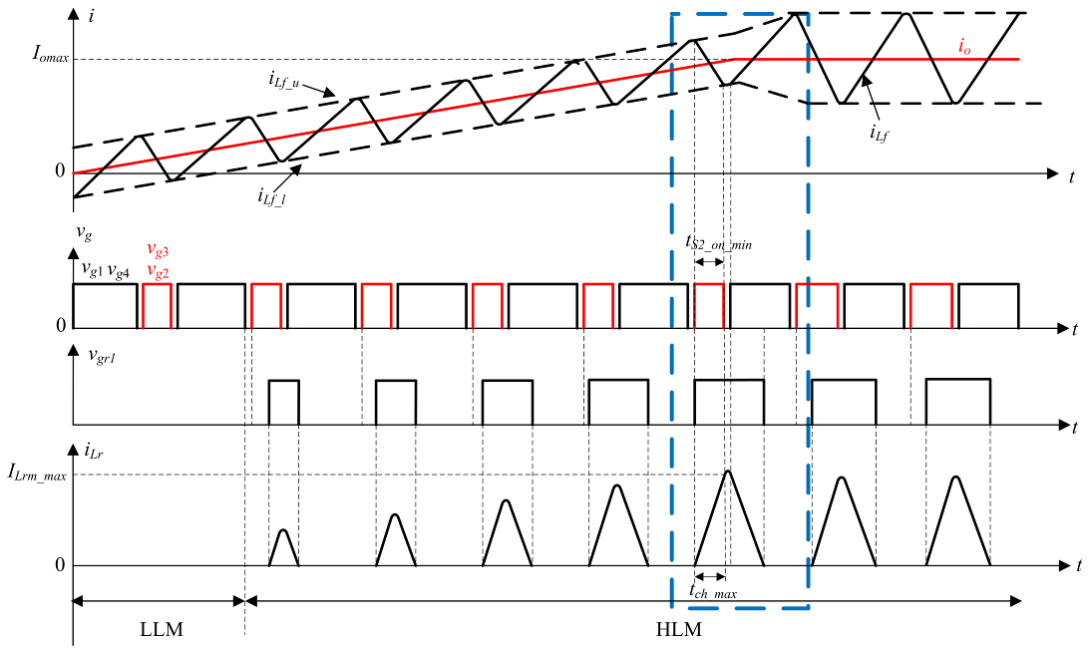

Fig. 8. Dynamic response waveforms when the output current increases from zero to the maximum value.

where ξ_c is the system-damping factor usually ranging from 0.5 to 0.9, and Z_o is the load impedance.

The damping factor is selected as $\xi_c = 0.707$, and in the DC output, the load impedance is set as $Z_o = R_o = 3.7\ \Omega$, which is shown in Table II. The filter ratio is selected as follows:

$$\sqrt{\frac{L_f}{C_f}} = 4 \tag{55}$$

From Equs. (53) and (55), the parameters of the LC filter can be obtained as 20.8 μH and 1.3 μF. In selecting the commonly used values, the inductance and capacitance are specified as $L_f = 22$ μH and $C_f = 1$ μF. In this case, the cut-off frequency is $f_{LC} = 33.9$ kHz.

Step 2) Design the resonant capacitors

During the turn-off period, the resonant capacitors can slow down the voltage change rate (dv/dt), reducing the turn-off loss and the EMI noise. However, a high capacitance reduces the linearity of the output current because of the long transitional time.

The dead time is usually limited to $t_{dead} < T_s/10$ for the consideration of linearity. In addition, the resonant time t_r must be shorter than dead time t_{dead} according to (25). Therefore, the resonant time is limited to $t_r < T_s/20$. Based on the aforementioned requirement, the maximum resonant time in this case is selected as $t_{r\_max} = 0.15$ μs, and I_{r_min} is selected as $I_{r\_min} = 2.5$ A. According to Equ. (26), the resonant capacitor is obtained as $C_r < 2.343$ nF. Thus, the capacitance is specified as $C_r = 2$ nF with a margin.

Step 3) Design the resonant inductor

During the charging and discharging times, the resonant inductor can slow down the current change rate di_{Lr}/dt, reducing the turn-on loss of the auxiliary switches and the EMI noise. However, a high resonant inductance leads to low D_{max} and DC-link voltage utilization because of the long on-time of the auxiliary circuit. Usually, the maximum charging time of the resonant inductor should meet the requirement $t_{ch\_mzx} < T_s/10$ for the consideration of DC voltage utilization. The maximum resonant time in this case is selected as $t_{ch\_max} = 0.4$ μs. In addition, the maximum initial resonant inductor current is usually higher than the output current. Thus, it is selected as $I_{Lrm\_max} = 1.5I_{o\_max} = 12$ A. According to Equ. (42), the resonant inductor is obtained as $L_r < 2.67$ μH. In this case, the inductance is specified as $L_r = 2.2$ μH.

TABLE II
PARAMETERS OF THE CIRCUIT

Parameter	Value
DC voltage V_s	80 V
Switching frequency f_s	200 kHz
Maximum output current I_{o_max}	8 A
Dead time t_{dead}	0.2 μs
Load	3.7 Ω, 4.87 mH
Filter inductor L_f	22 μH
Filter capacitor C_f	1 μF
Resonant inductor L_r	2.2 μH
Resonant capacitor C_r	2 nF

Thus, the parameters of the circuit are shown in Table II.

Step 4) Determine the initial resonant current I_r and maximal duty ratio D_{max}

In achieving NZVS, Inequalities (27) and (30) must hold. Based on the parameters in Table II, the initial resonant

TABLE III
COMPARISON OF THE PARAMETERS WITH THE TRADITIONAL AND PROPOSED CONTROLS

	Proposed control	Traditional control
D_{max}	0.879	0.868
η_{dc}	0.758	0.736
t_{ch_max}	305 ns	358 ns
I_{Lrm_max}	11.066 A	13 A

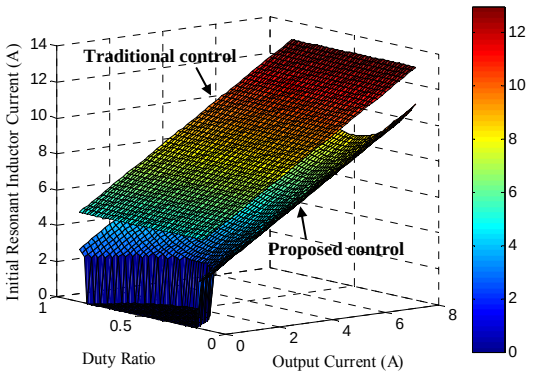

Fig. 9. Initial resonant inductor current of the improved ARSI with the traditional and proposed controls.

current must meet the following requirement.

$$I_r > 1.76\text{A} \tag{56}$$

The minimum initial resonant current is selected as I_{r_min} = 2.5 A. Therefore, when $i_{Lf\_l} < -2.5$ A and $i_{Lf\_u} > 2.5$ A, the inverter operates in the LLM according to Table I. Otherwise, the inverter operates in the HLM.

In achieving AZVS given by Equs. (29) and (31), the initial resonant current should satisfy the following condition.

$$I_r > 4.8\text{A} \tag{57}$$

Therefore, the initial resonant current in AZVS is selected as I_{r_A} = 5 A.

The parameters of the improved ARSI with the proposed and traditional controls are shown in Table III, which are obtained from Equs. (42)-(45). In achieving ZVS from zero load to full load, D_{max} must be less than 0.879, and the DC-link voltage utilization should be 0.758. Compared with that for the traditional control, the η_{dc} of the ARSI for the proposed control is increased by 0.022. The required maximum resonant inductor current I_{Lrm_max} is reduced by 1.934 A, and the maximum on time of resonant branch t_{ch_max} is shortened by 53 ns.

Fig. 9 shows the initial resonant current of the improved ARSI for the proposed and traditional controls when the output current is positive. When $i_{Lf_l} < -2.5$A, the ARSI for the proposed control operates in LLM, as shown in the deep blue area of Fig. 9. The resonant inductor current I_{Lrm} is 0 A. However, the I_{Lrm} of the ARSI for the traditional control is 5 A to 6 A to obtain the 5 A initial resonant current. In addition, the peak current of the resonant inductor for the proposed control is approximately 11 A, which occurs in the condition

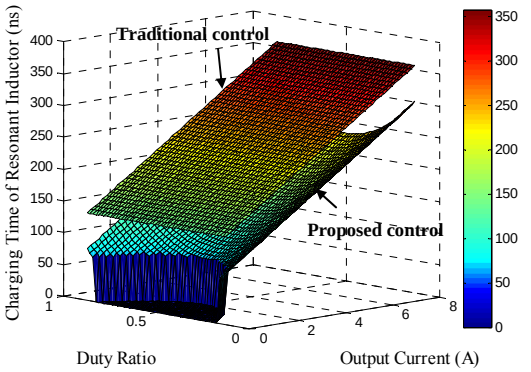

Fig. 10. Charging time of the resonant inductor of the improved ARSI for the traditional and proposed controls.

of the maximum output current and maximum duty ratio. For the traditional control, the peak current of the resonant inductor is 13 A. Therefore, the resonant inductor current I_{Lrm} of the ARSI for the proposed control is 2 A to 6 A less than that for the traditional control from zero load to full load.

A lower resonant inductor current I_{Lrm} results in a shorter charging time t_{ch}. Fig. 10 shows the charging time of the resonant inductor of the ARSI for the traditional control and proposed control. The deep blue area shows that the ARSI for the proposed control operates in LLM. The charging time of the ARSI for the proposed control is 50 ns to 125 ns less than that for the traditional control from zero load to full load.

V. SIMULATION AND EXPERIMENT

The proposed control method was implemented in the Altera Cyclone IV FPGA of a digitally controlled ARSI prototype with the parameters listed in Table II. The closed-loop control diagram is shown in Fig. 11. Double-loop regulation is used. The inner capacitor current loop is used to increase the damping of the system. The outer output current loop is used to control the load current. The gate signals of the main switches are generated with PWM. The duty ratio is limited to less than 0.879 obtained from Equ. (49).

For auxiliary switches, the envelope currents of the filter inductor i_{Lf_l} and i_{Lf_u} are calculated using Equs. (39)–(40). Next, the mode judgment generates the enable signal of the auxiliary switches based on Table I. Meanwhile, the charging time t_{ch} and the on time t_A of the auxiliary switches are calculated through Equs. (42) and (43), where t_r in Equ. (43) is replaced by t_{dead}. Thus, the enabled auxiliary switch is turned on t_{ch} before the corresponding main switches are turned off. For an instant, S_{r1} is turned on before S_2 and S_3 are turned off, and S_{r2} is turned on before S_1 and S_4 are turned off, according to Table I.

Fig. 12 shows the prototype, which consists of an FPGA (Altera Corporation EP4CE22E22C7N) control board, a switching power supply, a MOSFET driver, and a power circuit. In reducing overvoltage ringing caused by the slow

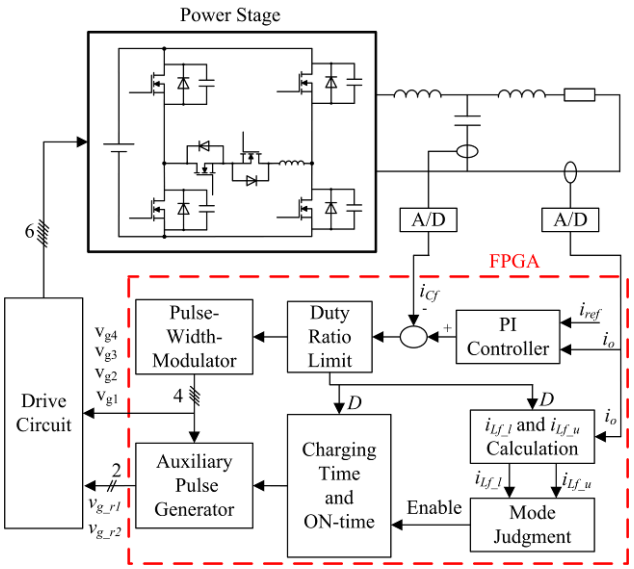

Fig. 11. Closed-loop control diagram of the improved ARSI.

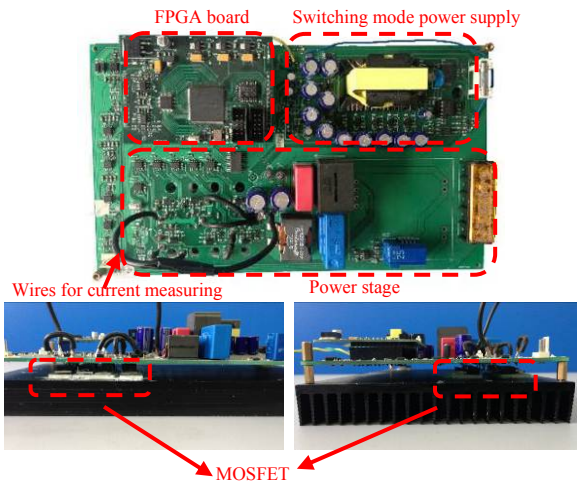

Fig. 12. Prototype.

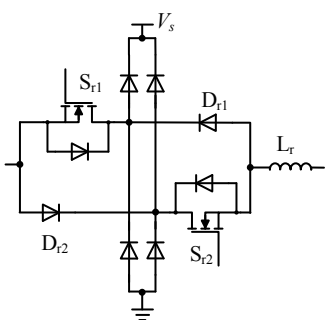

Fig. 13. Auxiliary circuit with the fast recovery diodes and clamping diodes.

reverse recovery of the intrinsic diodes, fast recovery diodes are used to block the body diodes of the auxiliary switches. Fig. 13 shows the auxiliary circuit with fast recovery diodes D_{r1} and D_{r2} and clamping diodes. The clamping diodes are used to address the overvoltage problem of the auxiliary switches caused by the parasitic components of the auxiliary circuit. The part numbers of the MOSFETs and diodes in the experiment are shown in Table IV.

TABLE IV
PART NUMBERS OF THE SEMICONDUCTOR COMPONENTS IN THE EXPERIMENT

Component	Part number
S_1-S_4	IRFB4227
S_{r1} and S_{r2}	IRFB4020
D_{r1} and D_{r2}	IDH06SG60C

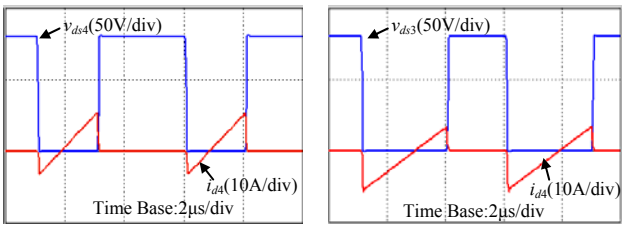

(a) S_4. (b) S_3.

Fig. 14. Simulation waveforms of main switches S_3 and S_4 when the output current is i_o = 1 A in the LLM.

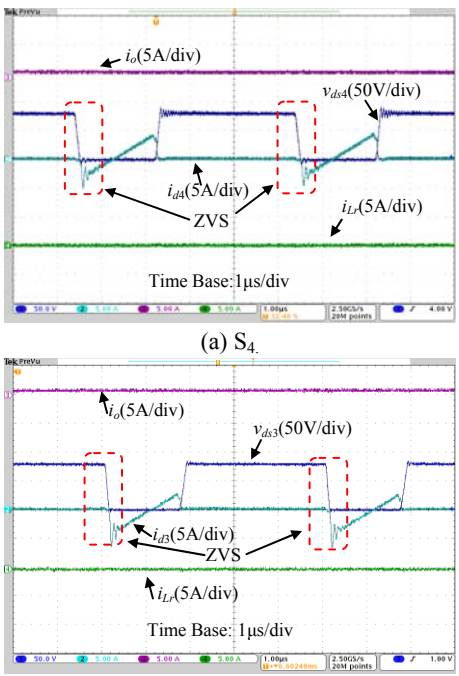

(a) S_4.

(b) S_3.

Fig. 15. Experimental waveforms of main switches S_3 and S_4 when the output current is i_o = 1 A in the LLM.

Fig. 14 and Fig. 15 show the simulation and experimental waveforms, respectively, of main switches S_3 and S_4 when the output current is i_o = 1 A in the LLM. The simulation is accomplished in Saber. The lower envelope of filter inductor current i_{Lf_l} is approximately –3 A, which is less than –2.5 A (the ringing is neglected.). Therefore, the auxiliary switches are not turned on, resulting in zero resonant inductor current. In addition, during the commutation time, the drain–source voltages across the MOSFETs v_{ds3} and v_{ds4} have already decreased to zero before their drain currents i_{d3} and i_{d4} have

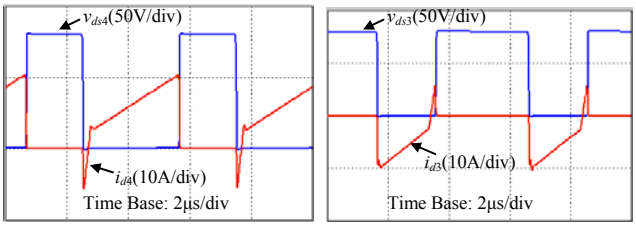

(a) S_4. (b) S_3.

Fig. 16. Simulation waveforms of main switches S_3 and S_4 when the output current is i_o = 8 A in the HLM.

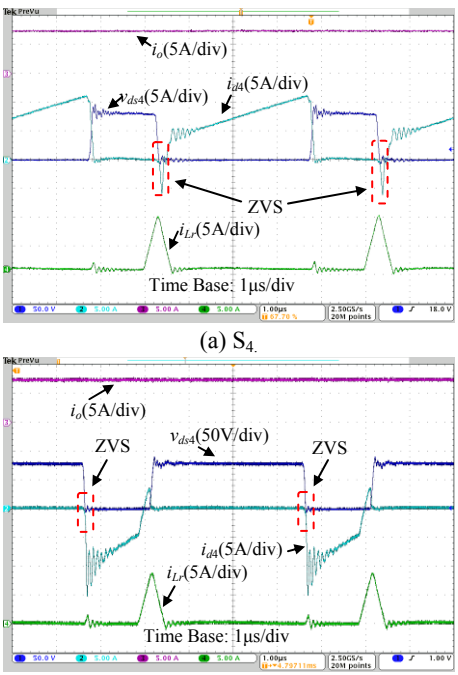

(a) S_4.

(b) S_3.

Fig. 17. Experimental waveforms of main switches S_3 and S_4 when the output current is i_o = 8 A in the HLM.

begun to increase. NZVS is achieved with the ripple of filter inductor current.

Fig. 16 and Fig. 17 show the simulation and experimental waveforms, respectively, of main switches S_3 and S_4 when the output current is i_o = 8 A in the HLM. During the commutation time, S_3 achieves NZVS without the operation of the auxiliary circuit, whereas S_4 achieves AZVS by turning on S_{r1}.

Fig. 18 shows the simulation and experimental waveforms of auxiliary switch S_{r1}. i_{d_r1} and v_{ds_r1} do not overlap, resulting in zero switching loss. Thus, S_{r1} achieves ZCS.

Fig. 19 and Fig. 20 show the simulation and experimental waveforms, respectively, of the auxiliary current with an 8 A, 100 Hz sinusoidal output current. The experiments of the ARSI for the proposed and traditional controls are tested under the same conditions and the same parameters. The initial resonant current of AZVS is fixed at 5 A. The auxiliary resonant branch of the proposed control is not operated in the LLM with 0 A resonant inductor current in Fig. 19(a) and 20(a), whereas the auxiliary circuit is operated from zero load

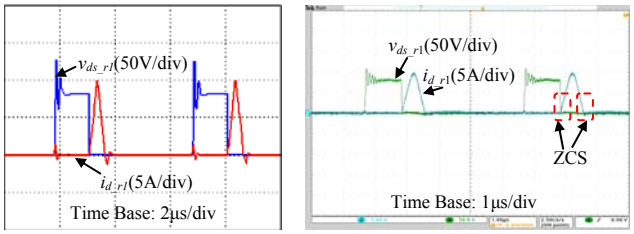

(a) Simulation. (b) Experiment.

Fig. 18. Waveforms of auxiliary switch S_{r1} when the output current is i_o = 8A in the HLM.

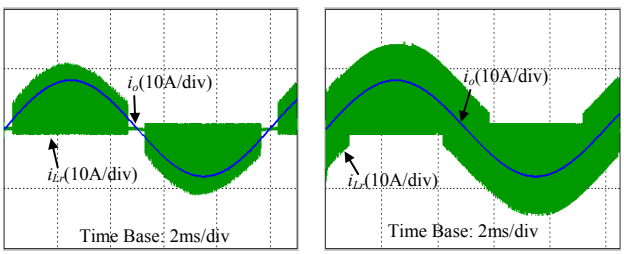

(a) Proposed control. (b) Traditional control.

Fig. 19. Simulation waveforms of the auxiliary current with an 8 A, 100 Hz sinusoidal output current.

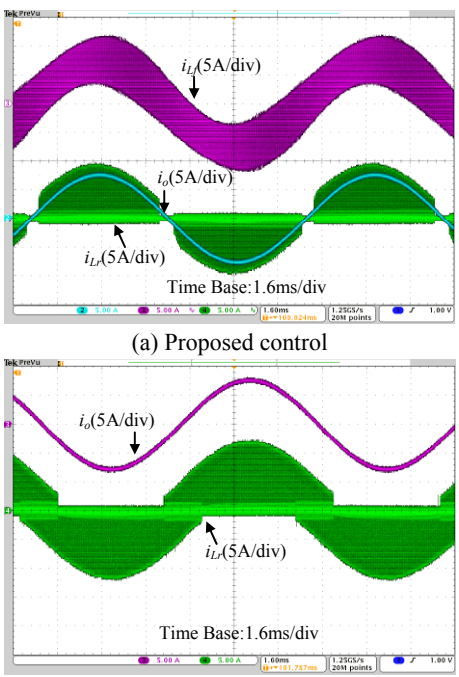

(a) Proposed control

(b) Traditional control

Fig. 20. Experimental waveforms of the auxiliary current with an 8 A, 100 Hz sinusoidal output current.

to full load for the traditional control shown in Fig. 19(b) and 20(b). In addition, in the HLM, the peak resonant inductor current follows the output current. When the output current is low, the resonant inductor current is also low.

Fig. 21 shows the initial resonant inductor current I_{Lrm} and charging time of resonant inductor t_{ch} for the theoretical calculation and the experimental results with an 8 A, 100 Hz sinusoidal output current. I_{Lrm} and t_{ch} of the ARSI for the proposed control are less than those for the traditional control

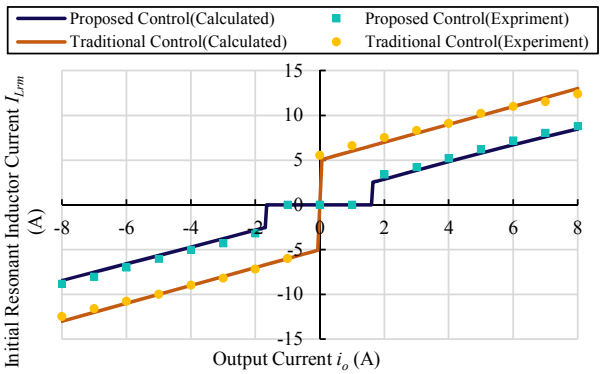

(a) Initial resonant inductor current.

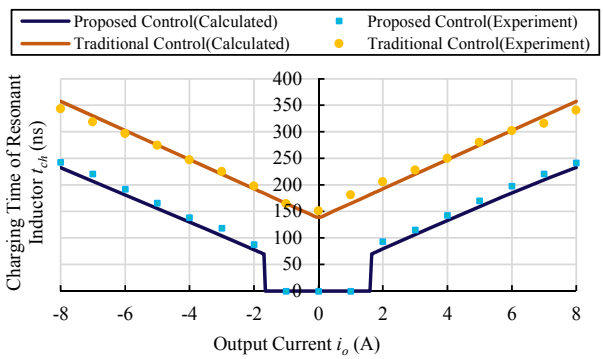

(b) Charging time of the resonant inductor.

Fig. 21. Initial resonant inductor current and the charging time of the resonant inductor with an 8 A, 100 Hz sinusoidal output current.

over the entire load range. When –1.5 A < i_o < 1.5 A, the ARSI for the proposed control operates in LLM. I_{Lrm} is 5–6.5 A less than that of the traditional control in the light load condition, and t_{ch} is 140–180 ns less. The peak initial resonant current is 8.84 A, occurring at 8 A output current, which is less than 12.4 A of the ARSI for the traditional control, whereas the maximum t_{ch} is 243.1 ns less than 343.75 ns of the ARSI for the traditional control. The experimental results are consistent with the theoretical calculation.

Fig. 22 shows the loss and efficiency comparison between the ARSI for the proposed control and the traditional control. Fig. 22(b) shows that the total loss increases with the output current. The loss of the inverter reaches up to 22.96 W at an 8 A output current for the proposed control, which is less than 28 W for the traditional control. Meanwhile, Fig. 22(b) shows that the efficiency of the proposed control is higher over the entire load range. The peak efficiency is 91.75%, occurring at an 8 A output current, which is higher than 89.73% for the traditional control.

Fig. 23 shows the distortion in the output current with an 8 A, 100 Hz sinusoidal output current in an open-loop configuration experiment. The red waveform is the FFT of the output current. The carrier harmonics of the inverter with the LC filter is approximately –66 dB, whereas that without

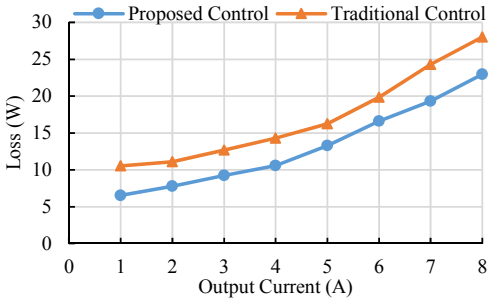

(a) Loss.

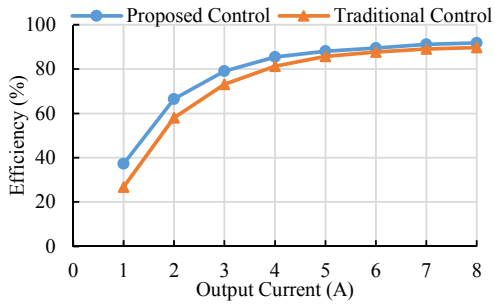

(b) Efficiency.

Fig. 22. Loss and efficiency comparison of the improved ARSI for the traditional and proposed controls.

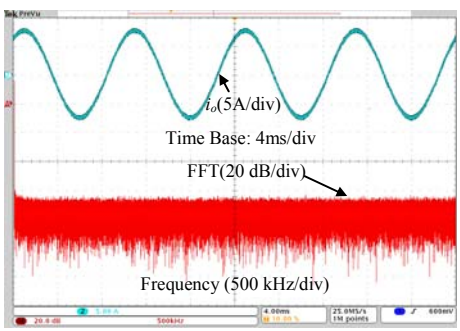

(a) With LC filter.

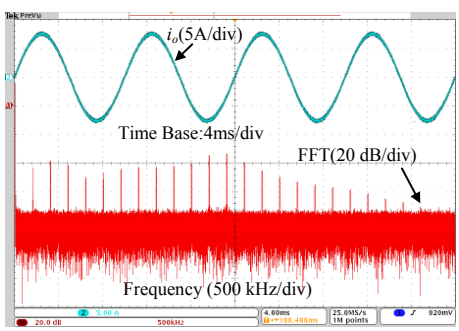

(b) Without LC filter.

Fig. 23. Distortion in the output current with an 8 A, 100 Hz sinusoidal output current

the LC filter is approximately –44 dB located at the first carrier harmonic (200 kHz). In addition, the other carrier harmonics are still large until the 21st carrier harmonics. With the addition of the LC filter, the carrier harmonics are greatly attenuated.

VI. CONCLUSIONS

A single-phase improved ARSI using an LC filter was proposed to reduce the output current ripple. Meanwhile, a novel load-adaptive control that considers and uses the filter inductor current ripple was proposed to address the extra auxiliary current problem of the traditional control implemented in the improved ARSI. The proposed ARSI operates in two modes: LLM and HLM. In the LLM, the main switches can operate at ZVS without the conduction of the auxiliary circuit. Some benefits are obtained from the improved ARSI for the proposed control as follows:

(1) The required auxiliary current is significantly reduced, especially in the LLM.
(2) The conduction loss is reduced, and the efficiency is improved because of lower auxiliary current.
(3) The DC-link voltage utilization is improved because of the shorter on time of the auxiliary circuit.

A prototype was developed to verify the effectiveness of the improved ARSI. The proposed inverter was found to successfully operate in LLM and HLM, achieving soft-switching from zero load to full load. When the output current is an 8 A, 100 Hz sinusoidal current, the initial resonant inductor current is 5–6.5 A less than that of the ARSI for the traditional control in the light load condition. The peak initial resonant current is 8.84 A at the output current of 8 A, which is less than the current of 12.4 A of the ARSI for the traditional control. By reducing the auxiliary current, the DC–link voltage utilization is improved from 0.736 to 0.758, and the peak efficiency at 8 A output current is improved from 89.73% to 91.75%. With the addition of the LC filter, the carrier harmonics are attenuated from –44dB to –66dB.

ACKNOWLEDGMENT

This study was supported by the State Key Program of National Natural Science of China under Grant 51537002.

REFERENCES

[1] R. M. Schmidt, G. Schitter, J. Eijk, *The design of high performance mechatronics*. Delft University Press, Chap. 5, 2011.
[2] A. Charalambous, X. Yuan, N. McNeill, Q. Yan, N. Oswald and P. Mellor, "EMI reduction with a soft-switched auxiliary commutated pole inverter," *IEEE Energy Conversion Congress and Exposition (ECCE)*, pp. 2650-2657, 2015.
[3] H. Zhu, J. S. Lai, A. R. Hefner, Y. Tang and C. Chen. "Modeling-based examination of conducted EMI emissions from hard and soft-switching PWM inverters," *IEEE Trans Ind. Appl.* Vol. 37, No. 5, pp. 1383-1393, Sep. /Oct. 2001.
[4] J. S. Lai, R. W. Young, "A delta-configured auxiliary resonant snubber inverter," *IEEE Trans. Ind. Appl.*, Vol. 32, No. 3, pp. 518-525, Jun. 1996.
[5] J. S. Lai, "Resonant snubber based soft-switching inverters for electric propulsion drives," *IEEE Trans. Ind. Electron.*, Vol. 44, No. 1, pp. 71-80, Feb. 1997.
[6] Q. Zhang, D. Zhang, H. Hu, J. Shen, and I. Bartarseh, "Controlled-type ZVS technique without auxiliary components for micro-inverters," *Journal of Power Electronics*, Vol. 13, No. 6, pp. 919-927, Nov. 2013.
[7] J. M. Schellekens, J. L. Duarte, H. Huisman, and M. A. M. Hendrix, "Fast shared current transient response in high-precision interleaved inverters," *IEEE Trans. Power Electron.*, Vol. 26, No. 11, pp. 3308–3317, Nov. 2011.
[8] W. McMurray, "Resonant snubbers with auxiliary switches," *IEEE Trans. Ind. Appl.*, Vol. 29, No. 2, pp. 355–362, Mar. 1993.
[9] A. Toba, T. Shimizu, G. Kimura, M. Shioya and S. Sano, "Auxiliary resonant commutated pole inverter using two internal voltage-points of DC source," *IEEE Trans. Ind. Electron.*, Vol. 45, No. 2, pp. 200-206, Apr. 1998.
[10] W. Yu, J. Lai, and S. Park, "An improved zero-voltage switching inverter using two coupled magnetics in one resonant pole," *IEEE Trans. Power Electron.*, Vol. 25, No. 4, pp. 952-961, Apr. 2011.
[11] R. C. Beltrame, J. R. Rakoski Zientarski, M. L. Da Silva Martins, J. R. Pinheiro, and H. L. Hey, "Simplified Zero-Voltage-Transition Circuits Applied to Bidirectional Poles: Concept and Synthesis Methodology," *IEEE Trans. Power Electronics*, Vol. 26, No. 6, pp. 1765-1776, Jun. 2011.
[12] J. Lai, W. Yu, P. Sun, S. Leslie, B. Arnet, C. Smith, and A. Cogan, "A Hybrid-Switch-Based Soft-Switching Inverter for Ultrahigh-Efficiency Traction Motor Drives," *IEEE Trans. Ind. Appl.,* Vol. 50, No. 3, pp. 1966-1973, May/June 2014.
[13] J. L. Russi, M. L. Da Silva Martins, and H. L. Hey, "Coupled-Filter-Inductor Soft-Switching Techniques: Principles and Topologies," *IEEE Trans. Ind. Electron.*, Vol. 55, No. 9, pp. 3361-3373, Sep. 2008.
[14] W. Yu, J. Lai, and S. Park, "An improved zero-voltage switching inverter using two coupled magnetics in one resonant pole," *IEEE Trans. Power Electron.*, Vol. 25, No. 4, pp. 952-961, Apr. 2010.
[15] K. Yi, S. Han, S. Choi, C. Kim, and G. Moon, "A simple ZVZCS sustain driver for a plasma display panel," *Journal of Power Electronics*, Vol. 6, No. 4, pp. 298-306, Oct. 2006.
[16] H. J. Yu, W. Dong, B. M. Song, and J. Lai, "Variable timing control for coupled-inductor feedback ZVT inverter," in *Proc. IEEE International Power Electronics and Motion Control Conf.*, pp. 1138-1143, 2000.
[17] B. Kou, H. Zhang and H. Zhang, "A High-precision control for a ZVT PWM soft-switching inverter to eliminate the dead-time effect," *Energies*, Vol. 9, No. 8, Jul. 2016.
[18] C. Chan, K. Chau, D. Chan, J. Yao, J.-S. Lai, and Y. Li, "Switching Characteristics and Efficiency Improvement with Auxiliary Resonant Snubber Based Soft-Switching Inverters," *IEEE PESC*, pp. 429-435, 1998.
[19] H. Hayama and N. Hoshi, "Adjustable dead-time control scheme for single-phase rectifier with auxiliary resonant snubber circuit," *IEEE Energy Conversion Congress and Exposition*, pp. 2129-2135, 2011.
[20] T. Morohoshi, N. Hoshi, and J. Haruna, "Dead-time compensation scheme for adjustable dead-time controlled three-phase resonant snubber inverter," *IEEE Annual International Energy Conversion Congress and Exhibition*, pp. 836-841, 2013.
[21] H. Kim and S. Sul, "A novel filter design for output LC filters of PWM inverters," *Journal of Power Electronics*, Vol. 11, No. 1, pp. 74-81, Jan. 2011.

Hailin Zhang was born in Chongqing, China. He received his B.E. and M.E. degrees in Electrical Engineering from Harbin Institute of Technology (HIT), Harbin, China, in 2010 and 2012, respectively. He is currently working toward a Ph.D. degree in the Institute of Electromagnetic and Electronic Technology, HIT. His research interests include high-precision power amplifiers and soft-switching converters.

Baoquan Kou was born in Heilongjiang, China. He received his B.E. degree from Harbin Institute of Technology (HIT), Harbin, China, in 1992, his M.E. degree from Chiba Institute of Technology, Narashino, Japan, in 1995, and his D.E. degree from HIT in 2004.

From 2005 to 2007, he worked in the mobile station for the postdoctoral researchers of HIT. Since 2007, he has been a Professor of the School of Electrical Engineering and Automation, HIT. His research interests include electric drives of electric vehicles, linear motors and linear electromagnetic drives, control of power quality, and superconducting motors.

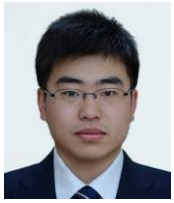

He Zhang was born in Heilongjiang, China. He received his B.E., M.E., and D.E. degrees from Harbin Institute of Technology (HIT), Harbin, China, in 2008, 2010, and 2015, respectively. Since 2015, he has been a Lecturer of the Department of Electrical Engineering, HIT. His research interests include magnetic levitation and linear and planar actuators.

Lu Zhang received his B.E., M.E., and D.E. degrees from Harbin Institute of Technology (HIT), Harbin, China, in 2008, 2010, and 2015, respectively. Since 2015, he has been a Research Assistant of the Institute of Electromagnetic and Electronic Technology, HIT. His research interests include long-stroke synchronous permanent magnet planar motors of high positioning accuracy and high response, linear motors, and torque motors.